CRYSTAL GROWTH & DESIGN
2006
VOL. 6, NO. 7
1663−1670

Studies on the Growth and Characterization of L-Asparaginium Picrate (LASP)—A Novel Nonlinear Optical Crystal

P. Srinivasan,[†] T. Kanagasekaran,[†] R. Gopalakrishnan,*[,†] G. Bhagavannarayana,[‡] and P. Ramasamy[§]

Department of Physics, Anna University, Chennai 600 025, India, Materials Characterization Division, National Physical Laboratory, New Delhi 110 012, India, and SSN College of Engineering, Kalavakkam 603 110, India

Received February 21, 2006; Revised Manuscript Received April 7, 2006

ABSTRACT: Good quality single crystals of L-asparaginium picrate have been grown by a low-temperature solution growth technique. The UV−visible−NIR absorption spectra were recorded for the grown crystal and relative second harmonic generation (SHG) efficiency was investigated to explore the NLO characteristics of the material for the first time in the literature. The relative SHG efficiency of the material is 66.5 times greater than that of KDP and 10 times higher than that of urea. The dielectric and mechanical behavior of the specimen were also studied. The structural perfection of the grown crystals has been analyzed by high-resolution X-ray diffraction (HRXRD) rocking curve measurements. Fourier transform infrared (FTIR) spectroscopic studies were also performed for the identification of different modes present in the compound.

Introduction

Nonlinear optical (NLO) materials utilize the nonlinear dependence of the refractive index on the applied electric field to bring forth other frequencies. The added esteem of nonlinear optical materials over lasers and electrooptics became preponderant from the early days of lasers. NLO materials endow the expansion of the circumscribed spectral regime of lasers. The pursuance of more efficient nonlinear optical (NLO) materials of increased optical quality is being goaded by the development of optical communication systems that require ultrafast broadband optical signal processing functions. The noetic construction of structurally controlled supramolecular assemblies (e.g., acentric and chiral solids) remains a great challenge even though the art of chemical synthesis of discrete molecules has significantly advanced in recent decades. The relevance of organic materials in this fresh context is because the delocalized electronic structure of π-conjugated organic compound offers a number of tantalizing opportunities in applications as nonlinear optical materials. Organic crystals in terms of nonlinear optical properties possess advantages when compared to their inorganic counterparts.[1−8] Also one of the advantages in working with organic materials is that they allow one to fine-tune the chemical structures and properties for the desired nonlinear optical properties.[9] In addition, they have large structural diversity. The properties of organic compounds can be refined using molecular engineering and chemical synthesis.[10] Hence they are projected as forefront candidates for fundamental and applied investigations. The design of organic polar crystals for quadratic NLO applications is supported by the observation that organic molecules containing π electron systems asymmetrized by electron donor and acceptor groups are highly polarizable entities.[11] Donor/acceptor benzene derivatives are sure to produce high molecular nonlinearity. An organic molecule should have large second-order hyperpolarizability (β) to exhibit good nonlinear optical properties. Extension of benzene derivatives has permitted an increase in the number of π electrons as well as their delocalization length, so as to lead to prodigious enhancement in β. Picric acid forms crystalline picrates of various organic molecules through ionic and hydrogen bonding and $\pi-\pi$ interactions.[12] It is known that picric acid acts not only as an acceptor to form various π stacking complexes with other aromatic molecules but also as an acidic ligand to form salts through specific electrostatic or hydrogen bond interactions.[13] Bonding of electron donor/acceptor picric acid molecules strongly depends on the nature of the partners. The linkage could involve not only electrostatic interactions but also the formation of molecular complexes.[14]

Acentric molecules consisting of highly delocalized π electron systems interacting with suitably substituted electron donor and acceptor groups exhibit a high value second-order polarizability (β).[15] L-Asparaginium picrate (LASP) is one such π donor−acceptor molecular compound in which L-asparagine acts as donor and the picric acid as electron acceptor. Anitha et al. have reported the unit cell parameters of LASP.[16] However, to our knowledge no systematic studies of LASP have been made. Hence, in the present investigation we report for the first time the bulk growth, optical, mechanical, and dielectric studies, and second harmonic generation (SHG) properties of L-asparaginium picrate (LASP).

Experiment

LASP crystals were grown by a slow evaporation solution growth technique. Picric acid is less soluble in water, whereas L-asparagine shows more affinity toward solubility only in water. Equimolar quantities of the parent compounds picric acid (Loba Chemie, 99%) and L-asparagine (Loba Chemie, 99%) were dissolved in a mixture of acetone and water (1:1). The reaction is depicted in Scheme 1. On cooling of the solution, the salt was obtained by crystallization at low temperature (25 °C). The material was repurified from aqueous solution by the recrystallization process. The single-crystal growth of this material has been performed from solution. Selection of suitable solvents is very definitive for the growth of good quality single crystals.[17] The solubility of LASP in acetone and water (1:1) was assessed as a function of temperature in the range 30−55 °C. A thermostatically controlled vessel (100 mL) was filled with an aqueous solution of LASP with some undissolved LASP and stirred for 24 h. On the next day, a small amount of the solution was pipetted out, and the concentration of the solute was determined gravimetrically. Figure 1 shows the solubility curve for LASP. The title compound exhibits good solubility and a

* Corresponding author. Tel: +91-44-2220 3374. Fax: +91-44-2220 3160. E-mail: krgkrishnan@annauniv.edu; krgkrishnan@yahoo.com.
[†] Anna University.
[‡] National Physical Laboratory.
[§] SSN College of Engineering.

10.1021/cg060094+ CCC: $33.50
Published on Web 06/10/2006

Scheme 1. Reaction Mechanism of LASP

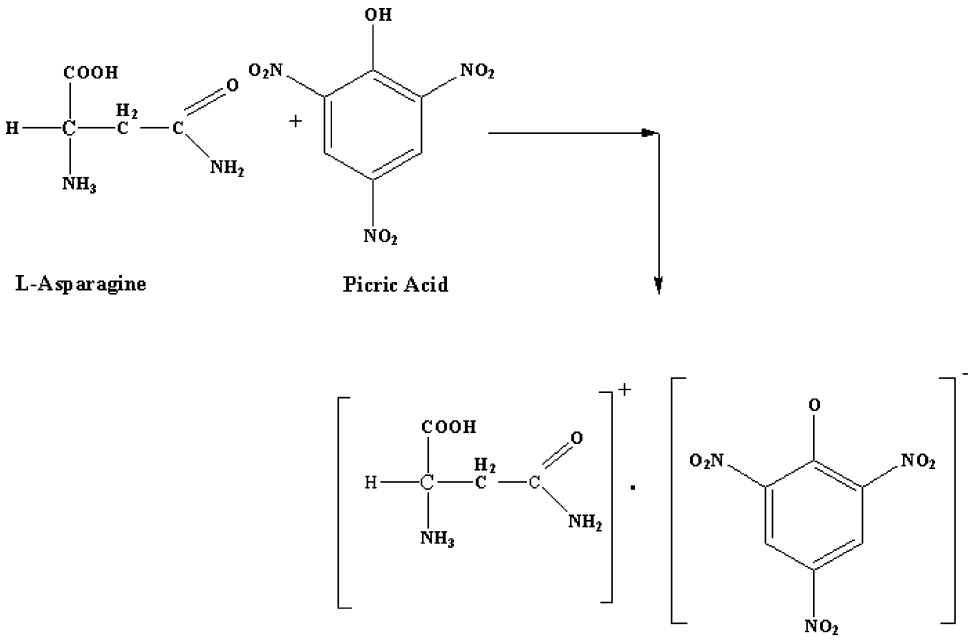

positive solubility−temperature gradient (direct solubility) in the mixed solvent of acetone and water (1:1). Thus, single crystals of LASP have been grown from saturated solution (pH = 2.01) of the synthesized salt of LASP by the slow evaporation technique at 30 °C using a constant-temperature bath having a control accuracy of (±0.01 °C). Yellowish crystals of size 1.5 × 0.8 × 0.4 cm^3 have been obtained (Figure 2).

X-ray diffraction data were collected at room temperature using a single-crystal X-ray diffractometer (ENRAF NONIUS CAD4, Mo Kα, $\lambda = 0.710\,69$). High-resolution X-ray diffraction analysis was carried out to study the structural perfection of LASP. A multicrystal X-ray diffractometer (MCD) developed at NPL (National Physical Laboratory, New Delhi),[18] set in (+,−,−,+) configuration, has been employed using Mo $K\alpha_1$ radiation originated from a fine focus sealed tube X-ray generator (Philips, 1743; 2 kW). The dispersive (+,−,−) configuration for the three Si(111) monochromator crystals of MCD has a special advantage to get a highly monochromatic ($\Delta\lambda/\lambda \leq 10^{-5}$) and collimated (horizontal divergence <3 arc sec) exploring beam ($K\alpha_1$).[19] The sample (0.8 × 0.2 × 0.2 cm^3) was lapped and polished and the resultant damaged surfaces were removed by preferential chemical etching using acetone and water in 1:1 ratio. The specimen occupies the fourth crystal stage and is oriented for diffraction in symmetrical Bragg geometry and (+,−,−,+) configuration of the diffractometer.

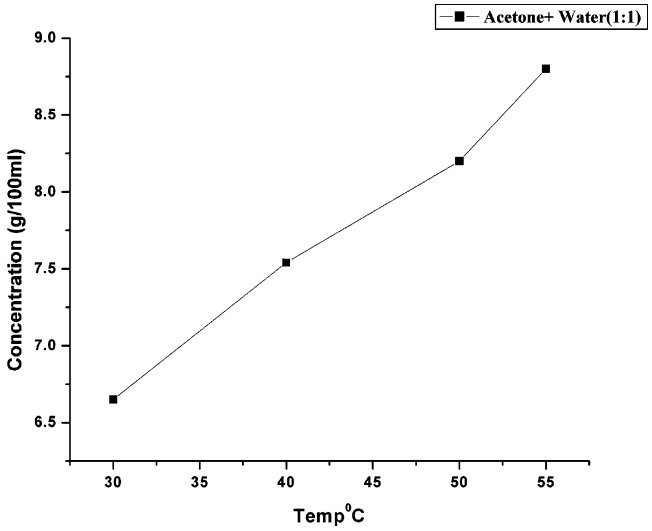

Figure 1. Solubility graph of LASP.

Dielectric properties are correlated with the electro-optic property of the crystals.[20] Carefully discerned samples of LASP were cut and polished on a soft tissue paper with fine grade alumina powder (0.1 μm) dispersed in a mixture of acetone, water, and DMFO (1:1:4). Each sample was electroded on both sides with silver paste (air-drying) to make the sample behave as a parallel plate capacitor. The dimensions of the crystal were measured using a traveling microscope (LC = 0.001 mm). The sample thickness was 0.4 to 1.4 mm. A HIOKI 3635 model LCR meter was used to measure the capacitance, dielectric loss (tan δ), and resistance of the sample as a function of frequency (range 30−95 °C). A small cylindrical furnace (20 cm × 20 cm × 20 cm), whose temperature was controlled by a Eurotherm temperature controller (0.01 °C) was used to house the sample. The dielectric constant was calculated by using the relation

$$\epsilon' = Ct/(\epsilon_0 A)$$

where ϵ_0 is the permittivitty of free space, t is the thickness of the sample, C is the capacitance, and A is the area of cross section. The conductivity of the crystal was calculated using the relation

$$\sigma_{dc} = t/(RA)$$

Quantitative measurement of relative efficiency of LASP with respect to well-known SHG materials KDP and urea was made by the Kurtz and Perry[21] powder technique. The finely powdered crystal of LASP was densely packed between two transparent glass slides. An Nd:YAG laser (DCR11) was used as a light source. A laser beam of fundamental

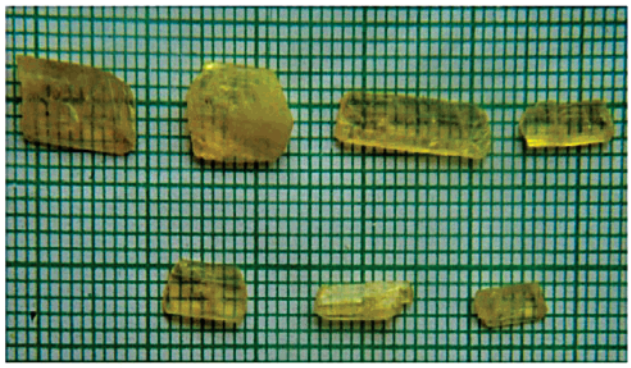

Figure 2. As-grown single crystals of LASP.

Table 1. LASP Crystal Shapes with Different Solvents

solvent	crystal shape
acetone + water (1:1)	block
ethanol + water (1:1)	plate-like
methanol + water (1:1)	small plates

wavelength of 1064 nm, 8 ns pulse width, with 10 Hz pulse rate was made to fall normally on the sample cell. The power of the incident beam was measured using a power meter. The transmitted fundamental wave was passed over a monochromator (Czerny Turner monochromator), which separates 532 nm (second harmonic signal) from 1064 nm, and absorbed by a $CuSO_4$ solution, which removes the 1064 nm light, and passed through BG-38 filter to remove the residual 1064 nm light and an interference filter with bandwidth of 4 nm and central wavelength of 532 nm. The green light was detected by a photomultiplier tube (Hamamatsu R5109, a visible PMT) and displayed on a storage oscilloscope (TDS 3052 B 500 MHz, Phosphor digital oscilloscope). KDP and urea crystals were powdered to the identical particle size and were used as reference materials in the SHG measurement. The melting point measurements were made using TEMPO PT s100-230 V melting point apparatus.

For optical device applications, the transparency in the near-IR region is significant rather than that in the visible region because 1.3 and 1.5 μm wavelengths are used in optical telecommunication systems.[22] The absorption spectrum for the title crystal was recorded using a Varian Cary 5E UV−vis−NIR spectrophotometer in the region 200−2000 nm.

The room-temperature mid-Fourier transform infrared spectrum of LASP was recorded in the region 400−4000 cm^{-1} at a resolution of ± 4 cm^{-1} by using a Perkin-Elmer Fourier transform infrared spectrophotometer (model SPECTRUM RX1), equipped with a $LiTaO_3$ detector, a KBr beam splitter, a He−Ne laser source, and a boxcar apodization used for 250 averaged interferograms collected for both the sample and the background. KBr pellets contained a fine LASP powder obtained from the grown single crystals.

The structure and composition of the crystalline solids are inviolably related to the mechanical hardness. Microhardness testing is one of the best methods of understanding the mechanical properties of materials such as fracture behavior, yield strength, brittleness index, and temperature of cracking.[23−24] Hardness of a material is a measure of resistance it offers to local deformation.[25] The hardness measurements were made on the prominent (301) plane of the crystal of thickness 0.3 cm using Leitz−Wetzler Vicker's hardness tester fitted with a Vicker's diamond pyramidal indenter and attached to an incident light microscope (Neophot-2 of Carl-Zeiss, Germany). Loads ranging from 0.5 to 5 g were used for making indentations, keeping the time of indentation constant at 10 s for all the cases. The diagonal lengths of the indentation mark and crack length were measured, using the micrometer eyepiece at a magnification of ×100. The microhardness value[25] was calculated using

$$H_V = \frac{(1.8544P)}{d^2}\ \mathrm{N/m^2}$$

where H_V is the Vicker's hardness number, P is the applied load (N), and d is the average diagonal length (m) of the indentation mark.

Results and Discussion

Good quality single crystals of LASP (Figure 2) were obtained using a mixed solvent of acetone and water (1:1). Other mixed solvents resulted in either plate-like or small crystals. The results are tabulated in Table 1.

The morphology of LASP establishes that there are six developed faces, out of which the {3 0 1} plane is more prominent. For each face, its parallel Friedel plane is also present in the grown crystal and shown diagrammatically in Figure 3. LASP belongs to the monoclinic crystal system with space group $P2_1$ having two molecules in the unit cell. The obtained unit cell parameters are in good agreement with the reported value.[16] Table 2 portrays the comparison between observed and reported

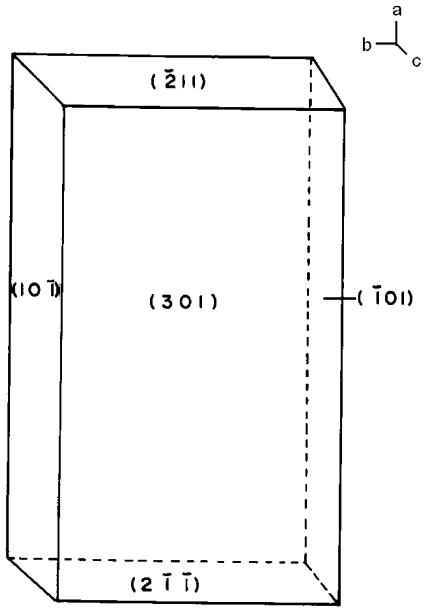

Figure 3. Morphology diagram of LASP.

Table 2. Comparison of Crystallographic Data of LASP

	reported[16]	present work
a, Å	10.367(4)	10.3322
b, Å	5.1611	5.1215
c, Å	13.120	13.0932
β (deg)	93.20	92.99

crystallographic data. Figure 4 shows the molecular structure of L-asparaginium picrate. The arrangement of picrate and asparagine ions shows that the title compound is an internally linked hydrogen bonded ion pair and hence can be regarded as a molecular crystal. The asymmetric unit of L-asparaginium picrate contains an asparaginium cation and a picrate anion where the carboxyl group is protonated. Thus a $\pi-\pi^*$ transition occurs in the carboxyl group, which gives rise to NLO properties in this system.[26] The picrate anion plays a pivotal role in hydrogen bonding (intermolecular hydrogen bonding) with the L-asparaginium residue and forms strong O−H···O and N−H···O hydrogen bonds.[16] The donor and acceptor molecules of L-asparagine and picric acid complex are held together by the contacts of van der Waals type. Hence, the effect of intermolecular hydrogen bonding between the phenolate ion of picric acid and the L-asparaginium residue will enhance the β value, which is the required property for a system to exhibit a nonlinear optical process. Table 3 summarizes the details of LASP.

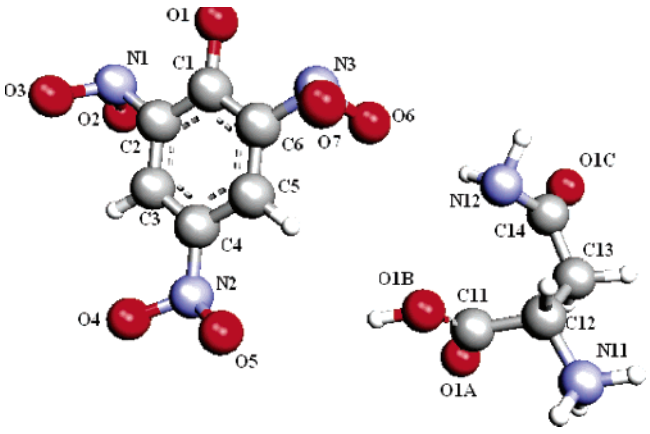

Figure 4. Molecular structure of LASP.

Table 3. Summary and Details of LASP Crystal

empirical formula	$C_4H_9N_2O_3^+C_6H_2N_3O_7^-$
formula weight	361.24
color	bright yellow
shape	black
size	$0.9 \times 0.4 \times 0.3$ cm^3
symmetry	monoclinic
space group	$P2_1$
unit cell parameters	$a = 10.3322$ Å, $\alpha = 90.3106°$
	$b = 5.1215$ Å, $\beta = 92.9924°$
	$c = 13.0932$ Å, $\gamma = 90.5880°$
volume (Å^3)	692.8445
Z	2
diffractometer	ENRAF NONIUS CAD 4
radiation	Mo Kα
wavelength	0.71069 Å
hygroscopicity	nonhygroscopic
UV absorption (cut off)	430 nm
mechanical properties	moderately hard.
melting point	223−226 °C

Figure 5 shows the rocking curve of LASP crystal recorded for (101) diffracting planes. The square points are experimental points. The curve bears two additional peaks with adjacent angles 40 and 12 arc sec away from the main peak. These two additional peaks may be attributed to very low angle boundaries whose tilt angles are 40 and 12 arc sec. The full width at half-maximum (fwhm) of the individual boundaries are in the range 18 arc sec. The peak is less sharp, and the half width of the low angle boundaries are 42 and 96 arc sec. From the HRXRD results, we elucidate that the incorporation of solvent into the growing crystal, which is common in solution grown crystals, is responsible for the very low angle boundaries, and we conclude that the quality of the crystal is good.

The results of dielectric measurements are shown in Figures 6 and 7. It can be reasoned out that the dielectric constant (ϵ') and dielectric loss (tan δ) decrease with increase of frequency. The large values of dielectric constant at low frequency suggest that there is a contribution from all four known sources of polarization, namely, electronic, ionic, dipolar, and space charge polarization. Space charge polarization is generally active at lower frequencies and high temperatures and indicates the perfection of the crystals.[27] Further, the space charge polarization will depend on the purity and perfection of the material. Its influence is large at higher temperature and is noticeable in the low-frequency region.[28] The changes of ϵ' and tan δ as a function of frequency for LASP may be considered as a normal

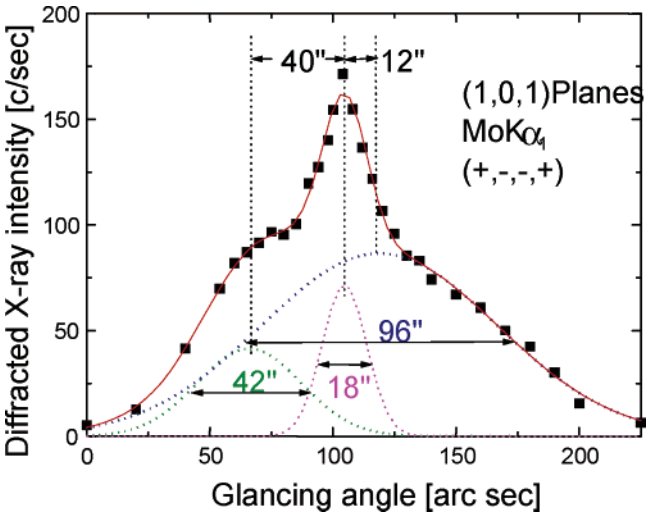

Figure 5. High-resolution X-ray diffraction (rocking curve) curve of LASP.

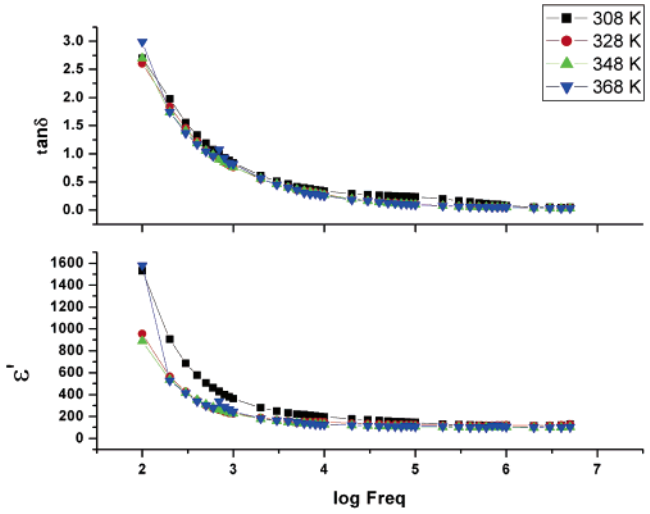

Figure 6. Plot of log(freq) vs dielectric constant and loss.

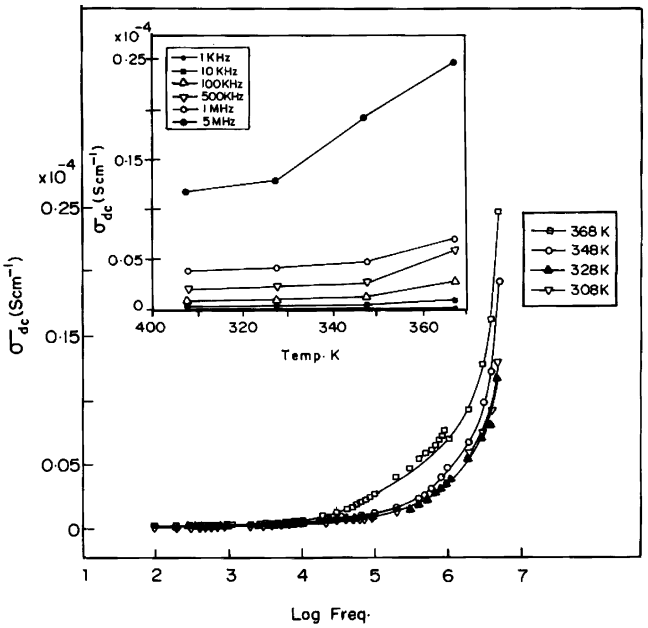

Figure 7. Log frequency vs conductivity of LASP.

behavior of a dielectric. The dielectric constant and dielectric loss decrease with increase in frequencies (Figure 6). The low value of dielectric loss (tan δ) indicates that the grown crystals of LASP are of reasonably good quality.[29] The dielectric constant of LASP crystal at 308 K (1 kHz) is 363, and this value decreases to 227 at 368 K. There is an ion−dipole interaction between dipole moments of the LASP molecule and the effective ionic charges. In the temperature range 308−368 K, the dielectric constant of dispersive medium decreases because the term contributing to dielectric constant from the ion−dipole interactions is compensated by the thermal energy leading to the relaxation of polarization.[28] Figure 7 shows the variations in dc conductivity (σ_{dc}) of LASP for different frequencies and different temperatures. At higher frequencies, the increased conductivity could be due to the reduction in the space charge polarization.[30] The increase in conductivity at higher frequencies for a given temperature confirms small polaron hopping in the title crystal.[31−33] The conductivity of LASP increases upon increase in temperature. The electrical conduction in dielectrics is mainly a defect controlled process in the low temperature region. We ascertain from Figure 7 that

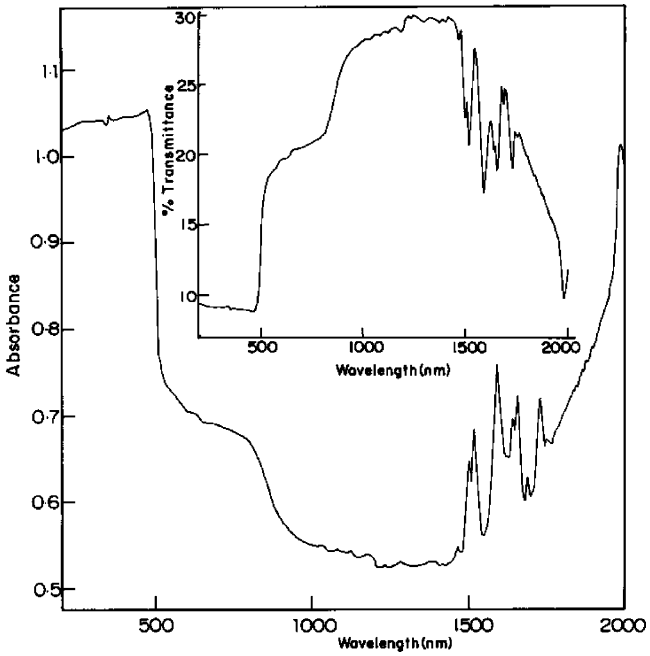

Figure 8. UV−vis−NIR spectrum of LASP.

the electrical conductivity of LASP is low at low temperature owing to trapping of some carriers at defect sites. At any particular temperature, however, the Gibbs's free energy of a crystal is minimal when a certain fraction of ions leaves the normal lattice. As the temperature rises, more and more defects are created, and as a result, the conductivity, which is predominantly due to the movement of defects produced by thermal activation, increases.[34]

Table 4 shows the comparison of SHG signal energy output for the title compound LASP with that for standard KDP and urea. It is clearly ascertained that LASP displays very high efficiency relative to KDP and urea counterparts and its parent compounds. The crystal is 66.5 times more efficient than KDP and 10 times more efficient than urea. The SHG efficiencies of the parent compounds were also studied and are included in Table 4. This strongly suggests the title compound as a potential candidate for SHG applications. The melting point of the title crystal was found to be 223−226 °C.

Table 4. Comparison of SHG Signal Energy Output

input power, mJ/pulse	KDP, mV	urea, mV	picric acid, mV	L-asparagine, mV	LASP, V
1.9	9.0		121	2	0.599
3.0		100	142	9	1.0

The UV−vis spectrum gives limited information about the structure of the molecule because the absorption of UV and visible light involves promotion of the electrons in the σ and π orbitals from the ground state to a higher energy state. The UV−vis−NIR spectrum of LASP is shown in Figure 8. When absorption is monitored from longer wavelength to shorter wavelength, enhanced absorption is observed between 1500 and 2000 nm. The absorption in this region is due to overtones of some fundamental vibrations of the nitro group in picric acid. There is low absorption at the fundamental wavelength (1064 nm) of the Nd:YAG laser, which contributes to the crystal's resistance to laser-induced damage. Further there is very little absorption at the wavelength of 532 nm, which can improve the second harmonic throughput.[35] The characteristic absorption band is observed at 430 nm, and there is no absorption band between 435 and 1400 nm; hence the crystal is expected to be transparent to all the UV−visible−NIR radiation between these two wavelengths.[36]

The FTIR spectrum of the compound is shown in Figure 9. The recorded FTIR spectra were compared with the standard spectra of the functional groups.[37] The hydrogen bond bridges two atoms that have higher electronegativity (such as O, N) than hydrogen. The hydrogen bonds most often found in nonlinear optical crystals of organics involve an interaction between a hydrogen bond to an sp^3 nitrogen or oxygen and an oxygen atom with more s-bond character although more symmetrical interactions also occur. The profound influences of hydrogen bonding will be different depending on whether the hydrogen bond is intramolecular or intermolecular and in the latter case on the specific extent and mode of interaction. The structure of LASP includes a weak intramolecular and a

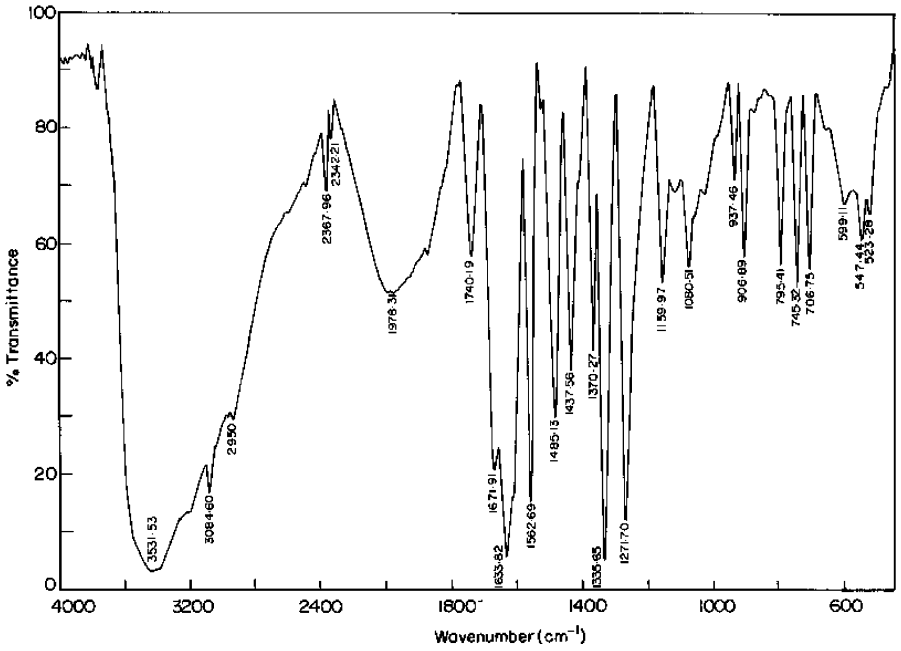

Figure 9. FTIR spectrum of LASP.

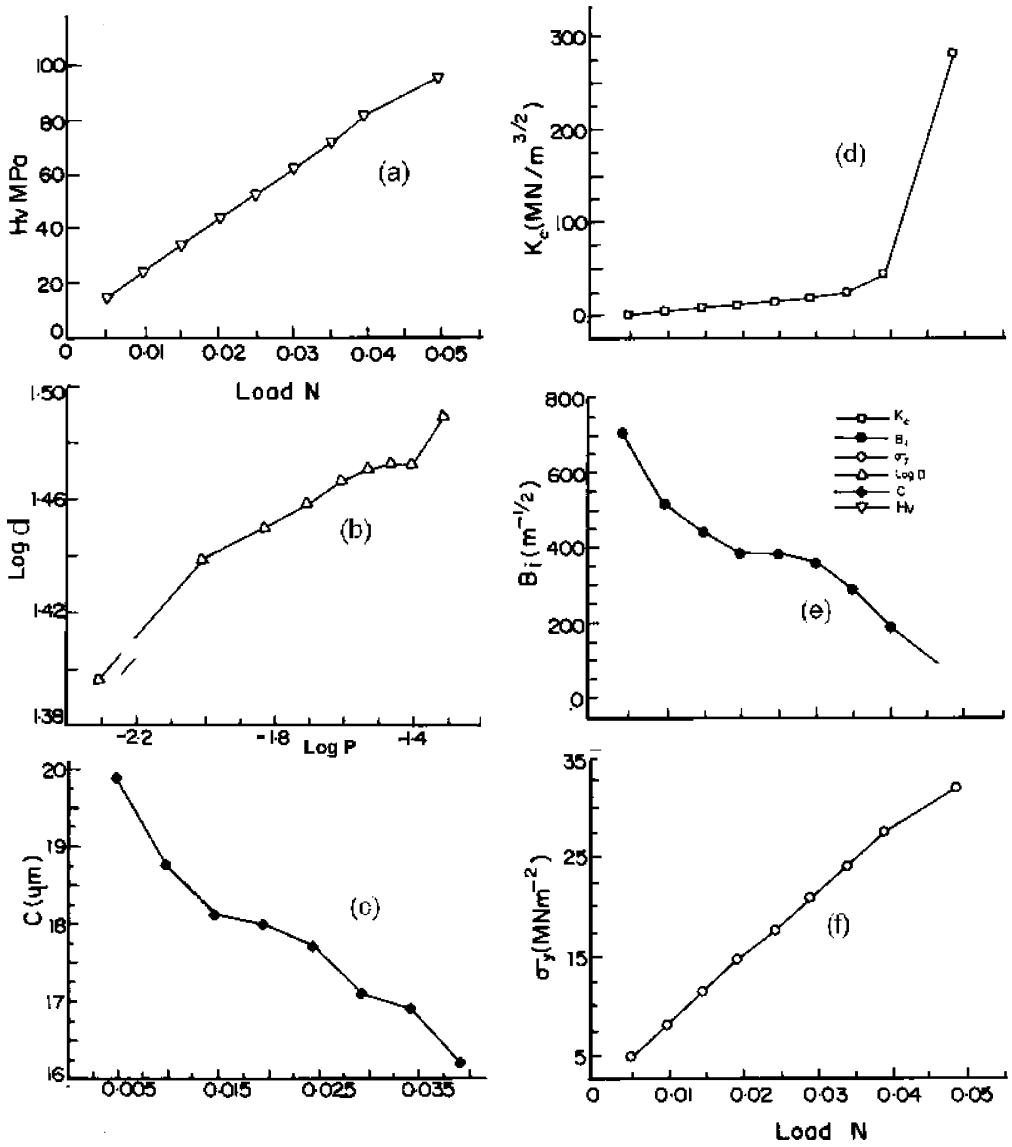

Figure 10. Mechanical behavior of LASP: (a) load vs hardness number; (b) log *P* vs log *d*; (c) load vs crack length; (d) load vs fracture toughness; (e) load vs brittleness index; (f) load vs yield strength.

strong intermolecular hydrogen bonding between the picrate anion and the L-asparaginium residue, which is characterized by O−H···O.[16] The frequency of such vibrations strongly depends on the length of those bonds. L-Asparagine exhibits tautomerism due to weak intramolecular hydrogen bonding between the OH group and the imine N atom. Due to tautomerism, the asparagine derivatives resemble urea, which is one of the very few organic materials in which second harmonic generation has actually been observed. In urea also, the hydrogen bonding polarizes the electron cloud and enhances the intramolecular nonlinear process. Vibrations of hydroxyl groups that are hydrogen bonded to aromatic ring π-electron systems absorb at 3670−3580 cm^{-1}.[38] In the present investigation, in LASP, the frequency of this band is shifted to low wavenumber region at 3531 cm^{-1} due to the addition of picric acid, which forms intermolecular hydrogen bonds with L-asparagine. The broad envelope between 2400 and 3700 cm^{-1} includes vibrations due to NH stretch (3200 cm^{-1}), aromatic CH stretch (3084.6 cm^{-1}), aliphatic CH stretch (about 2950 cm^{-1}), and broadening of OH stretch by hydrogen bonding. The less intense broad band at about 1978.3 cm^{-1} is due to a combination of NH_3^+ asymmetric bend and its torsional oscillation at 547.44 cm^{-1}. The peak at 1740.19 cm^{-1} is due to C═O stretch of COOH. The amide carbonyl stretch occurs at 1671.9 cm^{-1}. The asymmetric and symmetric modes of CO_2 occur at 1562.69 and 1437.56 cm^{-1}, respectively. The peak at 1485.13 cm^{-1} is assigned to NH_3^+ symmetric vibration. The symmetric stretch of NO_2 is assigned to the peak at 1335.65 cm^{-1}. The aliphatic CH bend appears at 1370.27 cm^{-1}. The OH bending modes produces peaks at 1271.7 and 906.89 cm^{-1}. The phenolic O vibration produces peak at 1159.97 cm^{-1}. From the above discussion, it is concluded that picric acid necessarily protanates the carboxyl group. The observed vibrational frequencies and their assignments are listed in Table 5.

A plot between the hardness number and the load is depicted in Figure 10a. We clearly infer that the microhardness number increases with increasing load. A plot (Figure 10b) obtained between log(*P*) and log(*d*) gives more or less a straight line. The relation connecting the applied load and diagonal length *d* of the indentor is given by Meyer's law $P = ad^n$. Here, *n* is the Meyer's index or work hardening coefficient that has been calculated from the slope of the straight line. The value of *n* obtained for LASP is 1.05. From careful observations on various materials, Onitsch[39] and Hanneman pointed out that *n* lies

Table 5. FTIR Spectral Data of LASP

wavenumber (cm^{-1})	assignments[a]
3531 s	intermolecular ν(O−H)
3084 s	aromatic ν(C−H)
2950 s	aliphatic ν(C−H)
2367 w	amino acid
1978 m	δas(NH_3^+)
1740 m	ν(C═O)
1671 s	amide ν(C = 0)
1633 s	δ(N−H)
1562 s	νas (COO)
1485 s	ν(NH_3^+)
1437 m	ν(COO)
1335 s	ν(NO_2)
1370 m	δ(C−H)
1271 s	δ(O−H)
1159 m	phenolic O
937 w	δC−N in plane
906 w	δC−N in plane
795 m	φNO_2
745 m	φNO_2
706 m	δring
599 m	νC−NO_2
523 m	ρNO_2

[a] ν, symmetric stretching; νas, asymmetric stretching; δ, bending; δas, asymmetric bending; ρ, rocking; φ, scissoring; s, strong; m, medium; w, weak.

between 1 and 1.6 for moderately hard materials, and it is more than 1.6 for soft materials. The value of n obtained is 1.05, which in comparison is harder than that of its parent compound picric acid ($n = 2.07$)[40] and benzimidazole ($n = 2.06$).[41] The term toughness may be defined as the property of the material by virtue of which it can absorb maximum energy before fracture takes place. The indendation impressions are usually seen associated with cracks at almost all loads. The presence of cracks confirms the decrease in microhardness.[42] For the title crystal, we see from Figure 10c that as load increases the crack decreases, which supports the increase in hardness of the material. The resistance to fracture indicates the toughness of the material. According to Ponton and Rawlings,[43] two types of crack systems can be formed in a material as a result of indendation. These are radial−median and Palmqvist crack systems. At a well-defined value of C/a, C being the crack length measured from the center of the indendation mark to the crack end and a being half the diagonal length of the indendation mark, transition from Palmqvist to median cracks occurs. For $C/a \leq 2.5$, the cracks developed are Palmqvist cracks. For the title crystal LASP, the type of crack obtained is Palmqvist. The pattern of Palmqvist crack is depicted in Figure 11. The fracture toughness K_c for median crack type is calculated using the relation[44]

$$K_c = kP/(al^{1/2})$$

where the constant $k = {}^1/_7$ for the Vicker's indentor and $l = C - a$ is the mean Palmqvist crack length. We see from Figure 10d that as the load increases the fracture toughness increases linearly up to 0.039 N and there is a steep increase in K_c for load 0.049 for LASP. Brittleness is an important property that affects the mechanical behavior of a material. It gives an idea about the fracture induced in a material without any appreciable deformation. The value of brittleness index, Bi, is calculated[45] using

$$\mathrm{Bi} = H_V/k_c$$

From the hardness value, the yield strength σ_y can be calculated.[46] For $n < 2$, the applicable formula is $\sigma_y = H_V/3$. We see from Figure 10e,f that the brittleness index and yield strength also increase as load increases. The increase in hardness accompanied by increase in fracture toughness, brittleness index, and yield strength are clearly seen.

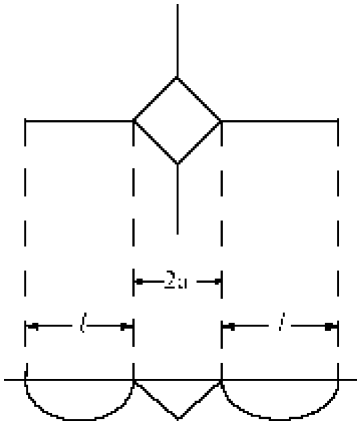

Figure 11. Geometry of Palmqvist crack around Vicker's indentation.

Conclusion

Optical quality single crystals of LASP were grown using a solution growth technique. The morphology unveils the growth habits of the material. The rocking curve measurements substantiate the good quality of the crystals. The occurrence of $\pi-\pi^*$ transition in the carboxyl group accounts for the nonlinearity in the title crystal. The dielectric constant and dielectric loss studies of LASP establish the normal dielectric behavior. The increase in conductivity may be attributed to a decrease in space charge polarization. The UV−vis−NIR spectrum elucidates that the crystal is transparent between 435−1400 nm. From the FTIR spectrum, we establish the presence of intermolecular hydrogen bonding, which could enhance the nonlinear property of the material. The hardness study projects the crystal to be moderately hard. The fracture toughness, brittleness index, and yield strength for LASP have been reported. The relative SHG efficiency of the material is 66.5 times greater than that of KDP and 10 times greater than that of urea. Based on these facts, it could be proposed that this novel material can be better accommodated for optical applications.

Detailed investigations of nonlinear characteristics of LASP are in progress and will be reported in due course.

Acknowledgment. The authors thank Dr. P. K. Das and Ms. Sampa Ghosh, Indian Institute of Science, Bangalore, for their support in SHG measurements.

References

(1) Newnham, R. E. *Structure−Property Relations*; Springer-Verlag: New York, 1975.
(2) Zyss, J. *Molecular Nonlinear Optics: Materials, Physics, and Devices*; Academic Press: New York, 1993.
(3) Agulló-López, F.; Cabrera, J. M.; Agulló-Rueda, F. *Electrooptics: Phenomena, Materials and Applications*; Academic Press: New York, 1994.
(4) Russell, V. A.; Evans, C. C.; Li, W.; Ward, M. D. *Science* **1997**, *276*, 575.
(5) Hierle, R.; Badamn, J.; Zyss, J. *J. Cryst. Growth* **1984,** 69, 545.
(6) Discoll, C. A.; Hoffmann, H. J.; Stone, R. E.; Perkins, P. E. *J. Opt. Soc. Am.* **1986**, *B31*, 683.
(7) Zyss, J. *J. Phys. D: Appl. Phys*. **1993**, *26*, 8198−8207.

(8) Desiraju, G. R. *Crystal Engineering: The Design of Organic Solids*; Elsevier: New York, 1989.
(9) Datta, A.; Pati, S. K. *J. Chem. Phys.* **2003**, *118* (18), 8420−8427.
(10) DeMatos, G.; Venkataraman, V.; Nogueria, E.; Belsley, M.; Criado, P. A.; Dianez, M. J.; Perez Garrido, E. *Synth. Met*. **2000**, *115*, 225.
(11) Pecaut, J.; Bagieu-Beucher, M. *Acta Crystallogr. C* **1993**, *49*, 834.
(12) Yamaguchi, S.; Goto, M.; Takayanagi, H.; Ogura, H. *Bull. Chem. Soc. Jpn*. **1988**, *61*, 1026.
(13) In, Y.; Nagata, H.; Doi, M.; Ishida, T.; Wakahara, A. *Acta Crystallogr. C* **1997**, *53*, 367−369.
(14) Zaderenko, P.; Gel, M. S.; Lopez, P.; Ballesteros, P.; Fonseco, I.; Albert, A. *Acta Crystallogr. B* **1997**, *53*, 961.
(15) Oudar, J.; Hierle, R. *J. Appl. Phys*. **1977**, *48*, 2699.
(16) Anitha, K.; Athimoolam, S.; Rajaram, R. K. *Acta Crystallogr. E* **2005**, *61*, o1463−o1465.
(17) Sherwood J. N. *Pure Appl. Opt.* **1998**, *7*, 229.
(18) Lal, K.; Bhagavannarayana, G. *J. Appl. Crystallogr*. **1964**, *36*, 681.
(19) Bhagavannarayana, G.; Choubey, A.; Shubin, Yu. V.; Lal, K. *J. Appl. Crystallogr*. **2005**, *38*, 448−454.
(20) Boomadevi, S.; Dhanasekaran, R. *J. Cryst. Growth* **2004**, *261*, 70−76.
(21) Kurtz, S. K.; Perry, T. T. *J. Appl. Phys*. **1968**, *39*, 3798.
(22) Kaino, T. *J. Opt. A: Pure Appl. Opt*. **2000**, *2*, R1−R7.
(23) Lawn, B. R.; Fuller, E. R. *J. Mater. Sci.* **1975**, *9*, 2016.
(24) Westbrook, J. H. Report 58-RL-2033 of the G. E. Research laboratory, USA, 1958.
(25) Mott W. *Micro Indentation Hardness Testing*; Butterworths: London, 1956; p 206.
(26) Pal, T.; Kar, T.; Boceli, G.; Rigi, L. *Cryst. Growth Des.* **2004**, *4*, 743−747.
(27) Prasad, N. V.; Prasad, G.; Bhimasankaran, T.; Suryanarayan, S. V.; Kumar, G. S. *Indian J. Pure. Appl. Phys*. **1996**, *34* (5), 639.
(28) Smyth, C. P. *Dielectric behavior and structure*; McGraw-Hill: New York.
(29) Benet, C. J.; Gnanam, F. D. *Cryst. Res. Technol.* **1994**, *29*, 707.
(30) Jonscher, K. *J. Mater. Sci.* **1989**, *24*, 372.
(31) Adler, D. In *Solid State Physics*; Seitz, F., Tunbull, D., Ehrenreich, H., Eds.; Academic Press: New York, 1968; Vol. 21, p 193.
(32) Appel, J. In *Solid State Physics*; Seitz, F., Tunbull, D., Ehrenreich, H., Eds.; Academic Press: New York, 1968; Vol. 21, p 1.
(33) Austin, I. G.; Mott, N. F. *Adv. Phys*. **1969**, *18*, 41.
(34) Jain, S. C; Dahake, S. L. *Indian J. Pure. Appl. Phys*. **1964**, *2*, 71.
(35) Krishnakumar, V.; Nagalakshmi, R. *Spectrochim. Acta, Part A* **2004**, *60*, 2733−2739.
(36) Rao, C. N. R. *Ultraviolet and visible spectroscopy of organic compound*; Prentice Hall of India Pvt Ltd.: New Delhi, 1984.
(37) Socrates, G. *Infrared Characteristic Group frequencies*; Wiley-Interscience: Chichester, U.K., 1980.
(38) Socrates, G. *Infrared and Raman Characteristic Group Frequencies*, 3rd ed.; Wiley: New York, 2001.
(39) Onitsch, E. M. *Microskope* **1950**, *95*, 12.
(40) Srinivasan, P.; Gunasekaran M.; Kanagasekaran, T.; Gopalakrishnan, R.; Ramasamy, P. *J. Cryst. Growth* **2006**, *289*, 639−646.
(41) Vijayan, N.; Ramesh Babu, R.; Gopalakrishnan, R.; Ramasamy, P.; Harrison, W. T. *J. Cryst. Growth* **2004**, *262*, 490−498.
(42) Hays, C.; Kendall, E. G. *Metallography* **1973**, *6*, 275.
(43) Ponton, C. B.; Rawlings, R. D. *Br. Ceram. Trans. J.* **1989**, *88*, 83.
(44) Heck, I. C. *Magnetic materials and their Applications*; Butterworths: London, 1974; p 645.
(45) Daniel, F. W.; Dunn, C. G. *Trans. Am. Soc. Met.* **1949**, *41*, 419.
(46) Cahoon, J. P.; Broughton, W. H.; Katzuk, A. R. *Met. Trans*. **1971**, *2*, 1979.

CG060094+